Journal of Applied Polymer Science

Rapid Prototyping of a Miniaturized Electrospinning Setup for the Production of Polymer Nanofibers

Oriana M. Vanderfleet,[1] Christine M. Gabardo,[2] Fahim M. Naeem,[3] Jose M. Moran-Mirabal,[3] Leyla Soleymani[1,2]

[1]Department of Engineering Physics, McMaster University, Hamilton, Ontario, Canada L8S 4L7
[2]School of Biomedical Engineering, McMaster University, Hamilton, Ontario, Canada L8S 4K1
[3]Department of Chemistry and Chemical Biology, McMaster University, Hamilton, Ontario, Canada L8S 4M1
Correspondence to: J. M. Moran-Mirabal (E-mail: mirabj@mcmaster.ca) and L. Soleymani (E-mail: soleyml@mcmaster.ca)

ABSTRACT: Fabrication of polymeric micro/nanofibers with controllable size, density, orientation, and composition is required for their translation into functional devices and materials. Electrospinning (ES) is a frequently used fiber fabrication technique, where ES parameters such as the applied electric field strength, architecture of the setup, and solution composition are manipulated to control the fiber properties. Here, we present a bench-top method for fabricating miniaturized, integrated, and highly tunable ES setups based on shrinkable polymer substrates. We show that using a combination of numerical modeling and controlling different parameters in the ES setup, including the spinneret to collector distance, and spinneret and collector designs, it is possible to tune the density, alignment, and orientation of electrospun fibers. In this way, we have produced 300–600 nm wide poly(ethylene oxide) fibers arranged as nonwoven mats on planar electrodes, aligned fibers on electrode edges, and individual suspended fibers spanning gaps between collector electrodes. The ability to rapidly prototype ES setups should enable us to study the effects of spinneret–collector configurations on fiber morphology, distribution, and conformation and to aid in the development of miniaturized ES setups designed to serve specific applications. © 2014 Wiley Periodicals, Inc. J. Appl. Polym. Sci. **2014**, *131*, 40629.

KEYWORDS: fibers; nanoparticles; nanowires and nanocrystals; synthesis and processing

Received 8 December 2013; accepted 21 February 2014
DOI: 10.1002/app.40629

INTRODUCTION

Electrospinning (ES) is a well-established, facile, and inexpensive bench-top technique used to fabricate microscale to nanoscale fibers with a wide range of compositions and properties. In typical ES setups, strong electric fields are applied between a viscous polymer droplet resting on a conductive tip (spinneret) and a grounded collector plate. As the material in the polymer solution is ionized, the charge repulsion within the droplet coupled with the attractive force from the counter electrode cause the deformation of the droplet and leads to the formation of a Taylor cone, from which a jet of the polymer solution is extracted. The electrostatic force that pulls the jet toward the counter electrode, along with the whipping motion from the jet's instability, stretch and thin out the fiber and allow the solvent to evaporate, resulting in the deposition of solid nanofibers at the collector plate. This method is routinely used to fabricate high-density, randomly oriented nonwoven fiber mats using electric field strengths between 1 and 25 kV/cm and typical working distances of 1–25 cm.[1,2] Such fiber mats have been used in applications such as biosensing,[3] tissue engineering scaffolds,[4] filtration membranes,[5] and drug delivery systems.[6]

The deposition of fibers with programmable density, orientation, and alignment on the surface of a variety of substrates or in suspended configurations spanning gaps or trenches is essential to fabricating functional materials and devices. For example, fiber-like features are prevalent in the body and the extracellular matrix (ECM), which makes ES an attractive technique for the fabrication of scaffolds that mimic cellular microenvironments *in vivo*. In tissue engineering, scaffold structure can be critical for cellular organization and function, and major differences have been reported in the production of ECM when aligned or randomly oriented nanofibers are used for nerve regeneration.[7,8] Biosensors based on nanofibers also present great promise, as they offer large specific surface areas for loading biorecognition elements (e.g., enzymes, antibodies, and nucleic acid probes). This results in biosensors with enhanced signal-to-background

ratio, sensitivity, and specificity.[9,10] In electrical device fabrication, nanofibers have been used as etch masks to pattern metallic or semiconductive layers.[11] In addition, these materials have been used in field-effect transistor,[12] gas sensing,[13] and light-emitting[14] devices.

To address the need for developing fibers with controllable alignment, orientation, and density, multiple electrically and mechanically modified ES setups have been developed. One common method is to mechanically translate or rotate the collector plate to obtain arrays of aligned fibers.[15,16] Other methods based on static collectors rely on controlling the electromagnetic field exerted on the ES jet through the use of auxiliary electrodes to focus and steer the charged jet,[17,18] electromagnets,[19] collector electrode configurations featuring metallic frames or predefined voids capable of local electric field modulation,[20–23] or a combination of these modifications. Fiber mats, aligned fibers, and individual fibers can be successfully fabricated using these modified setups.

In addition to conventional ES setups, in the past few years, there has been significant interest in developing near-field ES (NFES). In this method, short spinneret–collector distances (0.5–3 mm) are used to achieve controllable ES by taking advantage of the liquid jet stable region and reducing the effect of jet instability. NFES setups typically incorporate sharp tips to produce fibers having submicrometer diameters.[24,25] Although multiple setups have demonstrated controllable deposition of nanofibers using NFES on planar and patterned collectors,[16,26–28] it remains a lengthy and resource-intensive process to implement NFES setups with custom collectors, spinnerets, and spinneret–collector separations. To overcome this limitation, we have developed a new low-cost and rapid method to create tunable, miniaturized, and integrated ES setups, where new spinneret collector assemblies are designed, fabricated, and implemented in a matter of hours. In this method, spinneret–collector assemblies are fabricated from shrinkable polymer substrates using a computer-assisted drawing (CAD) software-driven cutter, followed by patterning of metallic thin films using adhesive vinyl film masking.[29] The integrated ES system is then heat shrunk to reduce the electrode dimensions and to enhance their mechanical stability. This simple fabrication process allows us to quickly design and fabricate ES setups with various spinneret–collector separations, spinneret geometries, and collector electrode configurations. By tuning the spinneret–collector configurations of the miniaturized ES setups, we can also tune the fiber arrangement from nonwoven mats to aligned fibers and fibers spanning millimeter gaps. Although setups that are able to produce different fiber arrangements have been previously demonstrated,[30] the originality of this method stems from the fact that the ES setup used for the rapid production of nanofibers is fabricated using bench-top methods.

EXPERIMENTAL

Materials

Polyethylene oxide (PEO) with an average molecular weight of 300 kDa and fluorescein were purchased from Sigma Aldrich (Oakville, ON), and 99.8% acetonitrile and 95% ethanol were purchased from Caledon Laboratories (Caledon, ON) and Commercial Alcohols (Brampton, ON), respectively. Adhesive vinyl (FDC-4300) and prestressed polystyrene sheets (KSF50) were purchased from FDC Graphic Films (South Bend, Indiana) and Grafix (Maple Heights, OH), respectively.

Fabrication of the Miniaturized Electrospinning Apparatus

To create the tip/collector assembly, first, the desired layout of the tip/collector assembly and the pattern of the tip electrode were specified using CAD software such as Adobe Illustrator CS4. The apparatus layout (layout of the tip/collector assembly) was transferred to the adhesive vinyl-covered polystyrene sheet using a Robo Pro CE5000-40-CRP Vinyl Cutter (Graphtec America, Irvine, CA) by cutting through the vinyl and the polystyrene sheet. Following the creation of the desired layout in the CAD program, the cutter was programmed to pattern the vinyl film as a sputtering mask for creating the ES tip electrode. Once the desired cuts were complete on the vinyl, the vinyl-coated polystyrene sheet was removed from the cutter and then the vinyl mask covering the regions designed as tip electrodes was peeled off, and the remaining vinyl was used as a mask in the sputtering process. The collector plate layout and electrode pattern were defined using the same methods used for patterning the tip/collector assembly and tip electrode described above.

The tip/collector assembly and the collector plate were then sputtered with a 99.99% gold target (LTS Chemicals, Chestnut Ridge, NY) in the chamber of a manual planar magnetron sputtering system (Torr Compact Research Coater CRC-600, New Windsor, NY). Once 200 nm of gold was deposited on the polystyrene surfaces, the samples were removed from the chamber, and all remaining vinyl was peeled off. The ES tip/collector assembly was heated in an Isotemp Vacuum Oven (Fisher Scientific, Ottawa, ON) to 160°C to heat shrink the prestressed polystyrene, whereas the collector plate was kept unshrunk. The collector plate was then slid through the slits of the tip/collector assembly, effectively assembling the miniaturized ES apparatus. The location of these slits determined the tip to target separation, and ES assemblies with separations of 1, 2, and 3 mm were fabricated.

Device Modeling and Electric Field Simulations

The electric fields of the ES setups with different collector plate configurations were numerically modeled using the finite element analysis software COMSOL Multiphysics 4.2 (COMSOL, Burlington, MA). The electric field simulations were calculated based on the standard values for electric conductivity and relative permittivity of the materials used in the model. A free triangular mesh was used to discretize the two-dimensional models, with custom minimum element size of 0.1 μm and maximum element size of 480 μm. A potential of 2.1 kV was applied to the ES tip, and the gold-coated collector plate was grounded.

Fiber Fabrication

Fiber fabrication was performed using a 7.5% (w/w) solution of 300 kDa PEO in acetonitrile with a fluorophore additive. The fluorophore additive consisted of 10 m*M* fluorescein in 95% ethanol, and 40 μL of additive was added per every gram of the PEO solution. The ES solution was deposited on the spinneret using 1.0-mL tuberculin syringes with hypodermic 25-gauge needles (Terumo, Burlington, ON). Alligator clips were used to create an electric field by connecting the tip and the collector to

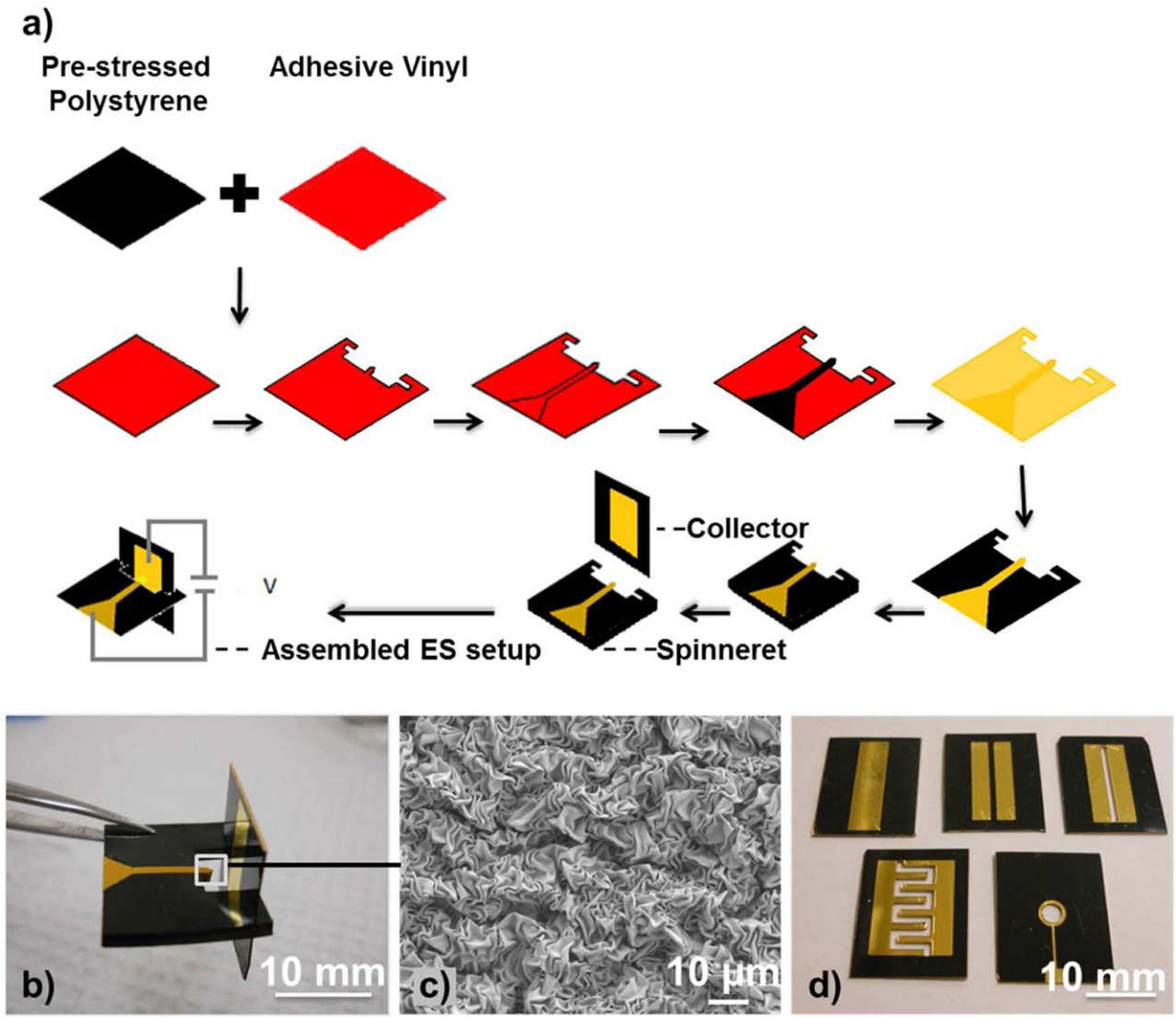

Figure 1. Bench-top fabrication technique for rapidly prototyping miniaturized ES setups. (a) The use of vinyl film masking and prestressed polystyrene sheet shrinking to produce collector and tip assemblies for ES apparatuses. (b) A miniaturized ES assembly. (c) Scanning electron micrograph of the gold surface after the PS shrinking process. (d) Various designs for the collector plate. [Color figure can be viewed in the online issue, which is available at wileyonlinelibrary.com.]

the positive and the negative terminals of the power (Spellman, Hauppauge, NY) supply and applying a voltage. Through these connections and by using tip/collector assemblies with desired tip-to-target separations, electric fields strengths of 7, 9, and 11 kV/cm were applied.

Fiber Characterization

The morphology, size, and orientation of the fibers were studied using fluorescence microscopy (Olympus BX51 upright fluorescent microscope), and scanning electron microscopy (SEM; JEOL JSM-7000F) was operated at 1.0 kV.

RESULTS AND DISCUSSION

The Miniaturized Setup and the Effect of Electrospinning Parameters

Our approach for fabricating a miniaturized ES setup is based on a versatile method developed in our laboratory[29] and is shown in schematic form in Figure 1(a). To create the miniaturized apparatus, CAD software is used to design the integrated tip/collector assembly and the collector plate. A bench-top craft cutter is first used to cut out designed areas of the polystyrene substrate that form the ES spinneret, the slits for inserting the fiber collecting plate, and an air gap between the spinneret and collector electrodes. After patterning the polystyrene substrate, the craft cutter is used to create vinyl masks for patterning the metal films that serve as the ES electrodes. A 200-nm-thick gold film is then sputtered onto the patterned vinyl covered tip/collector assembly and the collector electrode. After the deposition, the vinyl layer is lifted off and the tip/collector assembly is heated above the glass transition temperature of polystyrene to shrink the substrate. The smallest feature size that could be fabricated using the vinyl masking process is primarily controlled by motor step of the cutter used, and we found it to be 100 μm for

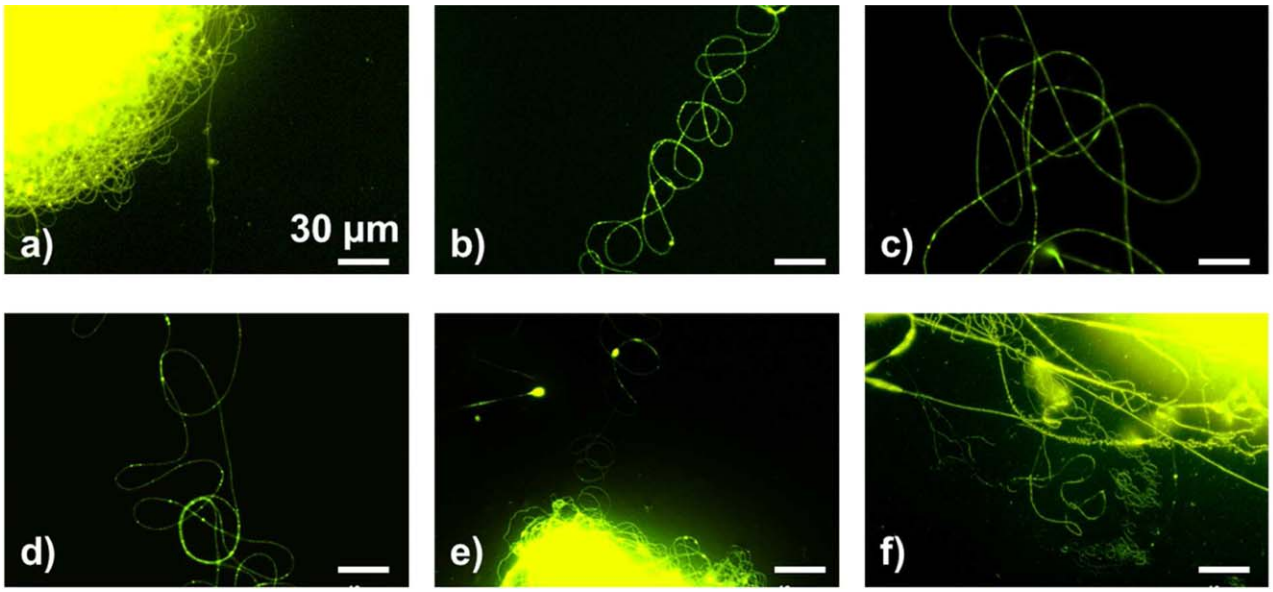

Figure 2. Fluorescence microscopy images of electrospun fibers on uniform gold collectors. ES was performed using a 7.5% (w/w) solution of 300 kDa PEO in acetonitrile at varying tip to collector distances (d_{tc}) and electric field strengths (E). (a) $E = 9$ kV/cm, $d_{tc} = 3$ mm; (b) $E = 9$ kV/cm, $d_{tc} = 2$ mm; (c) $E = 9$ kV/cm, $d_{tc} = 1$ mm; (d) $E = 7$ kV/cm, $d_{tc} = 3$ mm; (e) $E = 9$ kV/cm, $d_{tc} = 3$ mm; and (f) $E = 11$ kV/cm, $d_{tc} = 3$ mm. [Color figure can be viewed in the online issue, which is available at wileyonlinelibrary.com.]

straight features and 200 μm for circular features. Once shrunk, this translates to minimum feature sizes of about 40 and 80 μm for straight and circular features, respectively.[29]

Following the fabrication of the different components of the ES apparatus, the setup is assembled by sliding the collector plate through the slits of the tip/collector structure [Figure 1(b)]. To produce fibers, a droplet of solution is applied on the tip, followed by the application of a potential between the spinneret and the grounded collector. The resulting fibers are deposited on the collector plate. Our rapid fabrication technique provided the versatility that also allowed us to easily and inexpensively manufacture various collector plate configurations [Figure 1(d)]. The ability to alter the collector plate electrode geometry provided a simple method to tune the fiber orientation, without the need to incorporate additional equipment to rotate the collector.

To better understand the effect of the heat-induced shrinking of the polystyrene substrate on the structure of the spinneret electrode, we performed SEM on these electrodes. The SEM image in Figure 1(c) shows the structured gold surface of the spinneret, which has been previously reported. This type of structuring results when the prestressed polystyrene substrate shrinks causing the overlaying metallic thin film to wrinkle.[29] The microstructured gold film demonstrated better adhesion to the polystyrene substrate than a smooth, unstructured film when these two structures were qualitatively compared using the adhesive tape test: the unstructured film was removed after five consecutive peels, whereas the structured film was not visually changed through the peeling process.[29] This stable and robust ES spinneret featuring structured gold films could be used for many ES experiments (>10) without any visible deterioration.

The ES experiments were performed by dispensing a droplet of polymer solution onto the spinneret via a syringe and by biasing the ES setup as demonstrated in the last step of Figure 1(a). Optimal ES parameters were determined by adjusting the tip-to-target distance and the electric field strength. Each parameter was tested independently, and the resulting fibers were characterized using epifluorescence microscopy (Figure 2). First, the tip-to-target distance was varied while maintaining a constant electric field strength, PEO concentration, and solvent. An electric field strength of 9 kV/cm was chosen as it was the minimum electric field strength that allowed us to initiate a jet in an apparatus with a 1-mm spinneret to collector separation. Three tip-to-target separations were tested: 1, 2, and 3 mm. All three distances produced fluorescent fibers; however, fibers of different density were observed on collectors positioned at different distances from the spinneret [Figure 2(a)]. A working distance of 3 mm was chosen for subsequent experiments as it yielded the desired ES results with collectors containing many dense fiber mats and coils. Although fluorescence microscopy images are not suitable for quantitative fiber diameter measurements, as they typically lie below the resolution of the optical microscope (~300 nm), it is possible to see the trend of decreasing fiber diameter as the tip to collector separation is increased. This can be explained by the increased stretching at larger distances as the polymer jet travels from the tip to collector, and it is consistent with previous NFES studies.[25]

Next, electric field strengths of 7, 9, and 11 kV/cm were tested on apparatuses with spinneret-to-collector distances of 3 mm and with a 7.5% (w/w) solution of 300 kDa PEO in acetonitrile [Figure 2(d–f)]. At electric field strength of 11 kV/cm, the smallest visible fibers had diameters of ~600 nm, and the diameters appeared to vary significantly along the fiber lengths,

indicating an unstable ES jet. At 7 and 9 kV/cm, homogeneous fibers with diameters as small as ~300 nm (diffraction limit of the optical microscope) were visible, and many fiber coils were present on the collector plates. This demonstrates that consistent fibers with submicron diameters can be achieved with electric field strengths as low as 7 kV/cm. The electric field strength could not be further reduced because the ES process became inconsistent and many large micrometer-sized ribbons were produced. Thus, electric field strength of 7 kV/cm and a tip-to-target collector separation of 3 mm were chosen for the remaining modeling and experimental work to study the effect of collector electrode layout on fiber arrangement (Figures 3–5).

Electric Field Modeling

Next, we aimed to design a collector arrangement where individual straight fibers would span the distance between two collector electrodes. Previous studies have found that incorporating an insulating void between two grounded conductive electrodes on the collector plate resulted in the deposition of uniaxially aligned fibers across the gap.[21,22,31] This ES setup design has the advantage of not requiring any additional equipment to rotate the collector for obtaining aligned fibers. To better understand how an interelectrode-insulating void influences the electric field strength and direction, and the fiber deposition and alignment, two ES setups with different collector plate configurations were numerically modeled. The first collector design consisted of two parallel rectangular gold electrodes (3 mm wide, 16 mm long, and 200 nm thick) that were separated by a 1-mm polystyrene gap. The second collector design had the same electrode configuration; however, the polystyrene between the electrodes was removed creating an air gap. A 200 nm gold coating was placed on the walls of the air gap in the modeled geometry to approximate the architecture of devices fabricated using the methods illustrated in Figure 1. This approximation was made because we observed, using optical microscopy, that the device side walls within the air gap were covered with gold throughput their depths (data not shown). In the modeling work, a 2.1 kV potential was applied between the spinneret and the collector plates at a working distance of 3 mm, which matches the optimized spinneret–collector separation displayed in Figure 2.

Two-dimensional models of the ES device were created from a plane tangential to the spinneret and perpendicular to the gold surface of the collector. The field vectors—pointing in the direction of the electric field and having a length proportional to the field strength—were calculated and plotted in Figure 3(b) for both geometries. In addition, equipotential lines were calculated and plotted in Figure 3(b). The magnitude of the electric field in the lateral x-direction (E_x) was also plotted in Figure 3(c). The plots generated for both collector configurations [Figure 3(b)] demonstrate that the electric field vectors diverge from the positively biased tip electrode and converge toward the corners of the grounded collector electrodes. This suggests that charged fibers would be ejected from the tip electrode and electrostatically drawn toward the corners of the collector following the highest potential gradient and shortest distance to the collector electrodes.[32] Once a part of the fiber is immobilized on the collecting electrode, we expect the electrostatic interactions within the highly charged fibers and external electric fields exerted on these fibers to play a major role in positioning, stretching, and aligning the remainder of the fiber. It can be observed in Figure 3(c) that the collector having the air gap produces a higher magnitude of electric field in the lateral direction, E_x, within the void than the collector with the polystyrene filled gap. Pokorny et al.[33] have shown that there is a direct relationship between the strength of E_x and the degree of nanofiber alignment within a gap. Furthermore, this study concluded that tensional electrostatic forces that result from the enhanced horizontal electric field near the edges of the gap significantly influence fiber alignment. On the basis of our simulations and the previously reported results, we hypothesized that the air void would provide the preferred layout for the deposition of straight individual fibers spanning the gap between two electrode plates because of its higher laterally directed electric field.

To validate our modeling results and to test whether it would be possible to obtain individual stretched fibers within the air gap, we created an ES setup having the two collector configurations illustrated in Figure 3(a) and modeled in Figure 3(b,c). We biased the system by applying 2.1 kV to the spinneret and grounding the two collector electrodes as described previously with the optimal working distance of 3 mm. Representative fluorescence microscopy images of the two collectors featuring 1 mm polystyrene or air gaps are presented in Figure 3(d). From these images, it is evident that although fibers are present within the polystyrene gap [Figure 3(d, left)], these fibers change their orientations multiple times within the gap and it is not possible to get fully stretched and unidirectional fibers. In contrast, single, fully stretched, and unidirectional fibers were observed within the collectors having an air gap. This confirms our hypothesis that there is a correlation between the lateral electric field magnitude and the orientation of the fiber within the gap. These results are consistent with previous modeling and experimental studies where collectors with parallel edges and separated with air gaps were placed in planar or inclined configurations to divide electric field lines into two fractions for fabricating uniaxially aligned fibers. However, there are two differences between these fibers and the previously reported ones. The fiber density within the gap is significantly lower, and the fibers are not oriented at angle close to 90° to the electrode edges.[22,34] We suspect both of these differences to be caused by the nature of our ES setup, where a syringe is not used to continuously flow the ES solution through the tip. This results in a short ES duration that yields low-density or individual fibers within the gap. Using this method, we are able to create individual fibers at different orientations, which would enable us to study the mechanical, electrical, and optical properties of individual fibers to understand their possible anisotropic nature.

Collector Tunability

Multiple collector geometries were fabricated to demonstrate the versatility of this newly developed miniaturized ES system [Figure 4(a,d,g)]. Optimal parameters, including a 2.1 kV electric potential applied over a 3-mm separation, were used to perform ES experiments using these three collectors. To demonstrate that fabrication of individual and unidirectional fibers within air gaps is

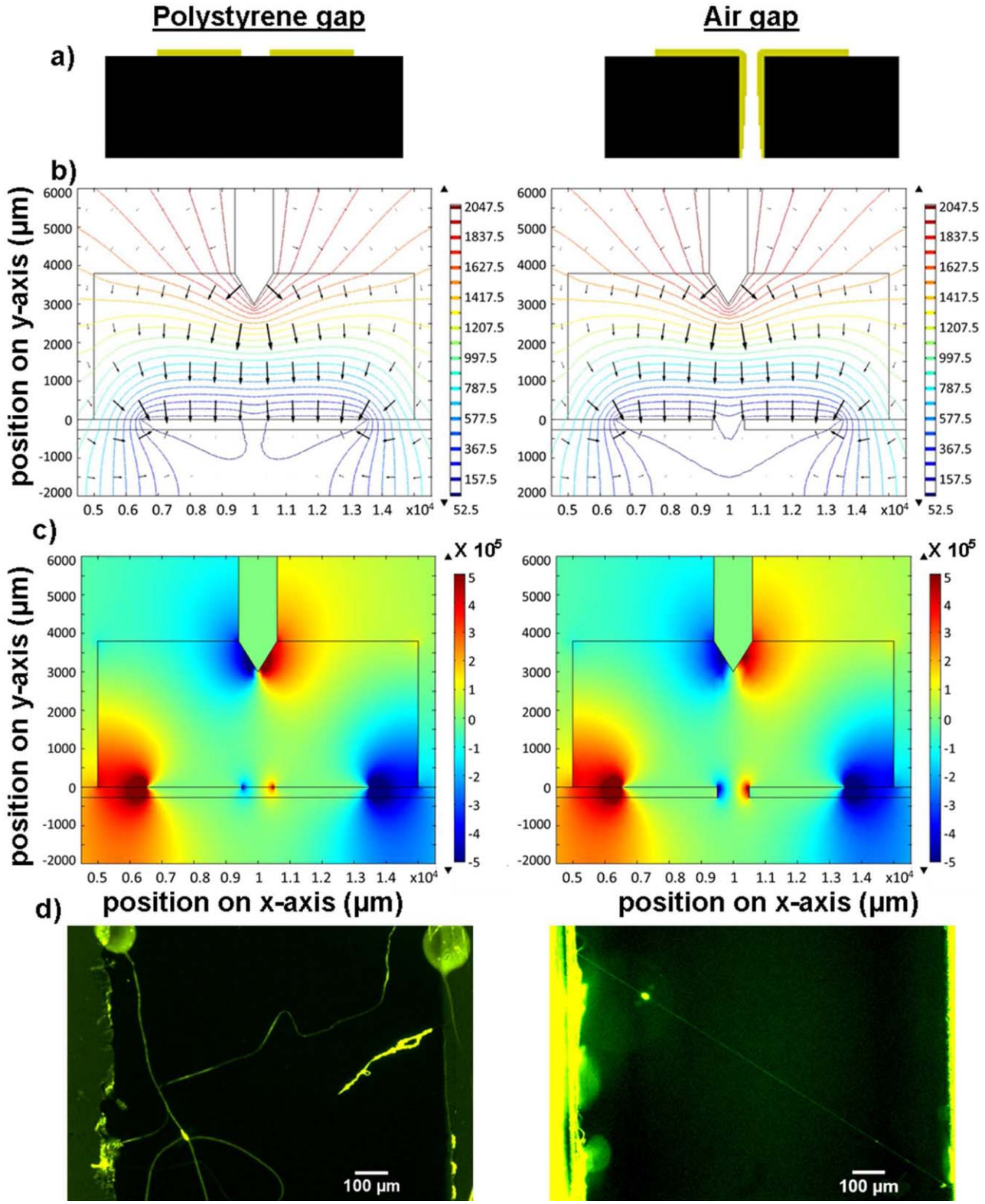

Figure 3. Theoretical and experimental comparison of collector plates with different dielectric materials within an interelectrode gap. (a) Schematic drawing of the collector plate electrodes with a polystyrene gap (left) and an air gap (right). (b) COMSOL simulation results demonstrating electric field vectors and equipotential lines (V) in a plane tangential to the spinneret and perpendicular to the collector for a polystyrene gap (left) and an air gap (right) device. (c) Plot of E_x magnitude (V/m) in the plane described in (b) for a polystyrene gap (left) and an air gap (right) device. (d) Fluorescence microscopy images of collector plates having a polystyrene gap (left) and an air gap (right). [Color figure can be viewed in the online issue, which is available at wileyonlinelibrary.com.]

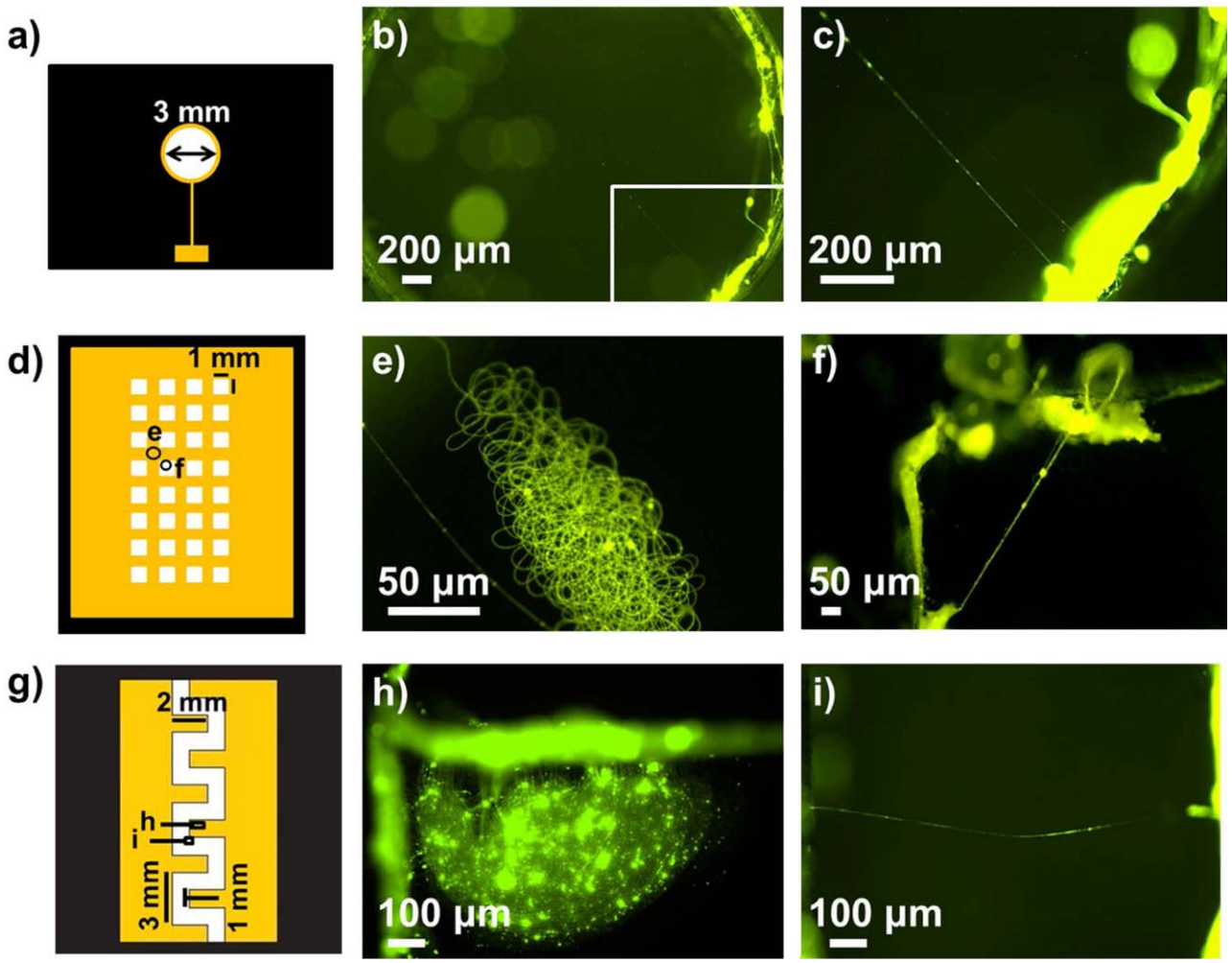

Figure 4. Electrospinning using the miniaturized ES setup with different collector layouts. (a) Schematic drawing of a collector with a ring electrode. (b) Fluorescence microscopy image of the air gap of the collector shown in (a). (c) Zoomed in image of the boxed area in (b). (d) Schematic drawing of a collector with a grid electrode. (e) Fluorescence microscopy image of the planar gold region of the collector circled in (d), and (f) the area within the air gap of the collector circled in (d). (g) Schematic drawing of a collector with interdigitated electrodes separated with an air gap. (h) Fluorescence microscopy image of the planar gold region of the collector circled in (g), and (i) the area within the air gap of the collector circled in (g). [Color figure can be viewed in the online issue, which is available at wileyonlinelibrary.com.]

not limited to collector electrodes with a rectangular geometry, we created collectors having the geometry of a single circular ring. For this purpose, a 3-mm-diameter circular opening was cut into the polystyrene substrate and a 0.5-mm gold ring was patterned along its edges. Fluorescence microscopy images [Figure 4(b,c)] demonstrate that this ES setup produced straight fibers spanning the entire 3-mm gap on the circular ring collector electrode. The methods described here for fabricating individual fibers within air gaps and interfaced with electrodes can be used to study the mechanical and electrical properties of new fiber materials.

In the study of our miniaturized ES setup, we achieved the fabrication of dense fiber mats using collector plates containing a single uniform electrode sheet [Figure 2(a)]. In addition, we obtained individual unidirectional fibers using collectors featuring an air gap [Figures 3(d, right) and 4(b,c)]. We sought to create a collector where a combination of fiber mats and individual fibers was deposited on different locations of the collectors. To this end, collectors featuring a metallic grid and collectors featuring interdigitated electrodes were created. In all cases, the dielectric material separating the electrodes was air. A grid pattern with 1×1 mm^2 air openings was used as a collector [Figure 4(d)] to obtain tunable fiber morphologies. Dense fiber mats were obtained on the gold surfaces between the air openings [Figure 4(e)], whereas individual fibers were obtained across the air gaps [Figure 4(f)]. This result is consistent with previous ES reports, where randomly oriented fibers were observed on conductive collectors, whereas uniaxially aligned fibers were present within air gaps.[34] An additional collector with an interdigitated pattern was used to deposit fibers with the developed miniaturized ES setup [Figure 4(g)]. Fiber mats with semicircular shapes were visible on the gold protrusions [Figure 4(h)]. In the center of the protrusion, the fibers were randomly oriented; however, along the edges of the protrusion, the fibers were oriented perpendicular to their

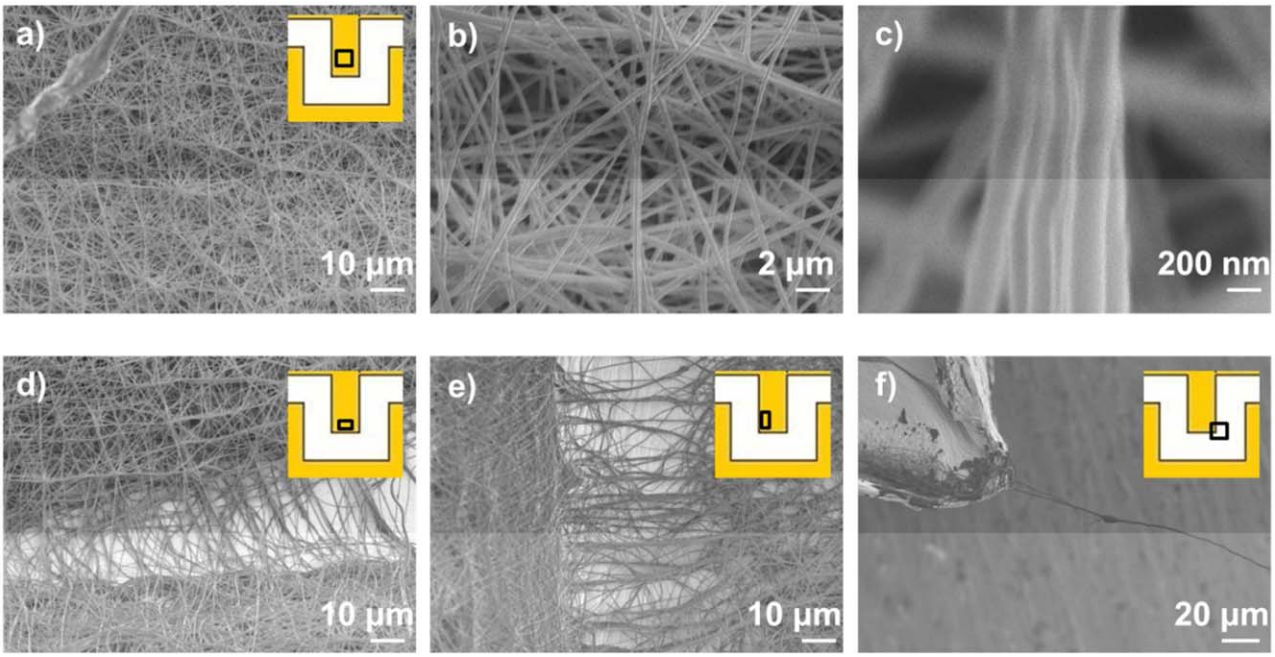

Figure 5. Scanning electron microscopy characterization of fibers deposited on the collector featuring the interdigitated electrodes from Figure 4(g). (a, d, e, and f) SEM micrographs of the region demonstrated in the figure insets. (b) Image of (a) at a higher magnification. (c) Image of (b) at a higher magnification. [Color figure can be viewed in the online issue, which is available at wileyonlinelibrary.com.]

outline. As expected, single straight fibers were observed within the air gaps separating the interdigitated electrodes. The results in Figure 4 show that the ES setups created using the newly developed bench-top fabrication method enable the production of nanofibers with tunable orientations, alignments, lengths, and densities. It is evident that planar sections of the collector electrodes are ideal surfaces for obtaining nonwoven fiber mats; however, air gaps between these metallic electrodes are ideal for obtaining individual fibers. In addition, fabricating fibers of varying lengths is possible by tuning the geometry and dimension of the air gap. The circular ring collector of Figure 4(a) yielded millimeter length fibers (bounded by the opening size and measured using calibrated imaging software), whereas the grid collector in Figure 4(d) produced submillimeter to millimeter sized fibers depending on their orientation within the air gap.

To better characterize the dimension and orientation of the fibers shown in Figure 4(h,i), we used SEM to image fibers deposited on the interdigitated collectors. Figure 5 shows representative SEM micrographs of the electrospun fibers at various positions on the interdigitated protrusions. Mats composed of randomly oriented fibers [Figure 5(a–c)] were visible in the middle of the semicircular mat shown in Figure 4(h). The fiber diameter within the mats and the corresponding standard deviation were calculated from 50 data points measured directly from SEM images (using the image analysis *software ImageJ*) to be 340 nm ± 60 nm. The fiber diameters fabricated here, using the newly developed horizontal and integrated setup, are similar to those observed by Sun et al. (300 nm), where a "dip-pen" NFES setup was used. The differences between the diameters seen can be explained as larger electric fields (10 kV/cm instead of 7.5 kV/cm) and smaller PEO concentration (5 wt % instead of 7.5 wt %) were used in the previous study.[24] Individual fibers were also visible in the air gap between protrusions [Figure 5(f)]. In addition to fiber mats and unidirectional individual fibers, we observed parallel, uniaxially aligned fiber networks with the fiber axis perpendicular to the protrusion's sides [Figure 5(d,e)]. We suspect this uniaxial alignment to be due to the component of the electric field perpendicular to the protrusion edges.

CONCLUSIONS

In summary, we have developed a new bench-top method for rapidly fabricating miniaturized ES setups with precise control over various parameters, including spinneret to collector distance, tip geometry, and collector electrode layout. Furthermore, we have shown that the tunability of the ES setup can be translated to controllable deposition of polymeric fibers, which can be arranged as fiber mats, individual fibers, or aligned fibers. The advantage of this NFES setup over the previously reported ones is that it is highly tunable and reproducible: it is possible to create identical or very different reusable or disposable setups in a matter of hours. We anticipate that the demonstrated miniaturized ES setup will find wide application in academic and industrial environments with a need for rapid and dynamic fiber-based prototyping.

ACKNOWLEDGMENTS

This study was supported by the NSERC Discovery Grant, the NSERC CREATE program, the NSERC USRA program, and the Science and Engineering Research Board at McMaster University. The authors thank Dr. John Preston for his support as the director of NSERC CREATE in Photovoltaics.

REFERENCES

1. Reneker, D. H.; Yarin, A. L. *Polymer* **2008**, *49*, 2387.
2. Doshi, J.; Reneker, D. H. *J. Electrostat.* **1995**, *35*, 151.
3. Wang, J.; Yao, H.-B.; He, D.; Zhang, C.-L.; Yu, S.-H. *ACS Appl. Mater. Interfaces* **2012**, *4*, 1963.
4. Yoshimoto, H.; Shin, Y. M.; Terai, H.; Vacanti, J. P. *Biomaterials* **2003**, *24*, 2077.
5. Gopal, R.; Kaur, S.; Ma, Z.; Chan, C.; Ramakrishna, S.; Matsuura, T. *J. Membr. Sci.* **2006**, *281*, 581.
6. Kenawy, E.-R.; Abdel-Hay, F. I.; El-Newehy, M. H.; Wnek, G. E. *Mater. Chem. Phys.* **2009**, *113*, 296.
7. Wang, H. B.; Mullins, M. E.; Cregg, J. M.; Hurtado, A.; Oudega, M.; Trombley, M. T.; Gilbert, R. J. *J. Neural Eng.* **2009**, *6*, 016001.
8. Lee, C. H.; Shin, H. J.; Cho, I. H.; Kang, Y.-M.; Kim, I. A.; Park, K.-D.; Shin, J.-W. *Biomaterials* **2005**, *26*, 1261.
9. Ren, G.; Xu, X.; Liu, Q.; Cheng, J.; Yuan, X.; Wu, L.; Wan, Y. *React. Funct. Polym.* **2006**, *66*, 1559.
10. Sawicka, K.; Gouma, P.; Simon, S. *Sens. Actuators B Chem.* **2005**, *108*, 585.
11. Ishii, Y.; Sakai, H.; Murata, H. *Thin Solid Films* **2009**, *518*, 647.
12. Pinto, N. J.; Johnson, A. T.; MacDiarmid, A. G.; Mueller, C. H.; Theofylaktos, N.; Robinson, D. C.; Miranda, F. A. *Appl. Phys. Lett.* **2003**, *83*, 4244.
13. Liu, H.; Kameoka, J.; Czaplewski, D. A.; Craighead, H. G. *Nano Lett.* **2004**, *4*, 671.
14. Moran-Mirabal, J. M.; Slinker, J. D.; DeFranco, J. A.; Verbridge, S. S.; Ilic, R.; Flores-Torres, S.; Abruña, H.; Malliaras, G. G.; Craighead, H. G. *Nano Lett.* **2007**, *7*, 458.
15. Pan, H.; Li, L.; Hu, L.; Cui, X. *Polymer* **2006**, *47*, 4901.
16. Zheng, G.; Li, W.; Wang, X.; Wu, D.; Sun, D.; Lin, L. *J. Phys. Appl. Phys.* **2010**, *43*, 415501.
17. Wu, Y.; Carnell, L. A.; Clark, R. L. *Polymer* **2007**, *48*, 5653.
18. Bellan, L. M.; Craighead, H. G. *J. Vac. Sci. Technol. B Microelectron. Nanometer Struct.* **2006**, *24*, 3179.
19. Yang, D.; Lu, B.; Zhao, Y.; Jiang, X. *Adv. Mater.* **2007**, *19*, 3702.
20. Ishii, Y.; Sakai, H.; Murata, H. *Mater. Lett.* **2008**, *62*, 3370.
21. Li, D.; Wang, Y.; Xia, Y. *Adv. Mater.* **2004**, *16*, 361.
22. Li, D.; Wang, Y.; Xia, Y. *Nano Lett.* **2003**, *3*, 1167.
23. Dersch, R.; Liu, T.; Schaper, A. K.; Greiner, A.; Wendorff, J. H. *J. Polym. Sci. Part A: Polym. Chem.* **2003**, *41*, 545.
24. Sun, D.; Chang, C.; Li, S.; Lin, L. *Nano Lett.* **2006**, *6*, 839.
25. Chang, C.; Limkrailassiri, K.; Lin, L. *Appl. Phys. Lett.* **2008**, *93*, 123111.
26. Ding, Z.; Salim, A.; Ziaie, B. *Langmuir* **2009**, *25*, 9648.
27. Bisht, G. S.; Canton, G.; Mirsepassi, A.; Kulinsky, L.; Oh, S.; Dunn-Rankin, D.; Madou, M. *J. Nano Lett.* **2011**, *11*, 1831.
28. Sahay, R.; Thavasi, V.; Ramakrishna, S. *J. Nanomaterials* **2011**, 2011, 1.
29. Gabardo, C. M.; Zhu, Y.; Soleymani, L.; Moran-Mirabal, J. M. *Adv. Funct. Mater.* **2013**, *23*, 3030.
30. Huang, Y.; Bu, N.; Duan, Y.; Pan, Y.; Liu, H.; Yin, Z.; Xiong, Y. *Nanoscale* **2013**, *5*, 12007.
31. Li, D.; Ouyang, G.; McCann, J. T.; Xia, Y. *Nano Lett.* **2005**, *5*, 913.
32. Hong, J. K.; Xu, G.; Piao, D.; Madihally, S. V. *J. Appl. Polym. Sci.* **2013**, *128*, 1583.
33. Pokorny, M.; Niedoba, K.; Velebny, V. *Appl. Phys. Lett.* **2010**, *96*, 193111.
34. Park, S. H.; Yang, D.-Y. *J. Appl. Polym. Sci.* **2011**, *120*, 1800.